J. Iron Steel Res. Int. (2019) 26:365–373
https://doi.org/10.1007/s42243-019-00237-7

ORIGINAL PAPER

Effects of silicon addition on optical properties of mould flux with iron oxide and estimation of apparent thermal conductivity of flux

Rie Endo[1] · Yo Kan[2] · Takashi Watanabe[1] · Miyuki Hayashi[1] · Masahiro Susa[1]

Received: 30 September 2018 / Revised: 10 January 2019 / Accepted: 17 January 2019 / Published online: 19 February 2019

Abstract
Mould flux with high absorptivity had been obtained in the reduction process of mould flux by silicon. For further utilisation of the mould flux with high absorptivity, the effect of silicon addition on the optical property has been investigated. The synthesised mould flux powder with iron oxide was melted with the addition of silicon powder at 1703 K followed by quenching, thus forming a glassy sample. After 5–30-min reduction, the samples exhibited black opaque colour. Meanwhile, the samples that were reduced for 45–60 min had a bluish grey colour. Many iron-based particles dispersed in the samples were micrometre order in diameter. To determine the effect of iron particles on the optical properties of the sample, extinction, scattering and absorption efficiencies were calculated according to Mie theory. Result showed that both scattering on the iron particle and absorption by iron effectively increase the extinction efficiency in the mould flux. Moreover, the silicon particle in the flux has large scattering efficiency. The black opaque colour is contributed by the existence of silicon and iron particles. The apparent thermal conductivity was calculated for the solid flux. Results also indicated that the entire glassy mould flux would effectively work for mild cooling in a continuous casting process owing to high absorptivity and small thermal conductivity.

Keywords Mould flux · Reduction · Iron oxide · Thermal conductivity · Optical property

1 Introduction

The productivity improvement of steels requires high-speed continuous casting. However, rapid casting is known to result in surface defects called longitudinal cracking owing to inhomogeneous solidification [1–4]. To avoid such defects, the steel is mildly cooled to render solidification homogeneity, which is the so-called mild cooling of the steel; that is, the heat from the steel shell is primarily transported through two mechanisms, namely conduction and radiation. The mould flux should be crystallised to reflect the strong radiation from molten steel, indicating that the decrease in radiative heat transfer is an effective technique to reduce heat flux from the steel shell. The crystallisation is generally promoted by the formation of cuspidine ($3CaO{\cdot}2SiO_2{\cdot}CaF_2$). However, conventional mould flux has several problems due to fluorine, that is, corrosion into facilities for continuous casting [5–7], submerged nozzle erosion [8, 9] and environmental pollution [10].

Meanwhile, iron oxides, which are natural contents in the mould flux, are reported to increase the radiative heat transfer across the crystallised flux because these components enhance the absorption of thermal emission from the steel shell [1]. Wang et al. [11] attempted to reduce the iron oxides in the current mould flux by adding 0.5–5.0% Si and maintaining the flux at 1703 K for 30 min. The mould flux was expected to have high reflectivity owing to the reduction product—metallic iron. However, all the produced mould flux exhibited a black opaque colour, which had low reflectivity but strong absorptivity, in both glassy and crystallised samples. This mould flux happened to be created, but another approach was suggested for the mild cooling, thus preventing the strong emissions from the steel shell by the mould flux with high absorbability. The

✉ Rie Endo
rie@mtl.titech.ac.jp

[1] Department of Materials Science and Engineering, Tokyo Institute of Technology, Tokyo 152-8552, Japan

[2] Department of Metallurgy and Ceramics Science, Tokyo Institute of Technology, Tokyo 152-8552, Japan

calculated radiative heat flux has the same magnitude as the conventional crystallised one. Moreover, this mechanism does not require crystalline phases, suggesting that the mould flux with high absorptivity has a potential for the fluorine-free flux.

The origin of the high absorptivity has not been investigated. Wang et al. [11] only mentioned that small metallic particles dispersed in the reduced flux, thus causing the strong absorption. Furthermore, they conducted the reduction only for 10 and 30 min. The previous understanding and evaluation of the colour stability are essential for the future utilisation of the reduced mould flux. Therefore, this study aims to investigate the relationship between the reduction time and subsequent microstructure, understand the optical property of the reduced mould flux based on the microstructure and evaluate the apparent thermal conductivity of the mould flux for further utilisation of the reduced mould flux.

2 Experimental

2.1 Samples

The base glass samples were partially prepared. The chemical composition of the base glass was the same as that used in the work of Wang et al. [11], that is, $w(Al_2O_3) + w(MgO) = 3.25$ mass%, $w(Na_2O) + w(F) = 19.7$ mass%, $w(Fe_2O_3) = 2.0$ mass% and $R = w(CaO)/w(SiO_2) = 1$, where R represents the basicity on the mass basis, including CaO originating from CaF_2. The compositions were determined on the basis of the mould flux for commercial use. The glass samples were synthesised from reagent-grade chemicals, namely CaO, SiO_2, Al_2O_3, MgO, Na_2O, CaF_2 and Fe_2O_3, where CaO was thermally decomposed from $CaCO_3$ at 1323 K for 43.2 ks and Na_2CO_3 was used to produce Na_2O. The reagent powders were mixed in an alumina mortar. The mixture was melted in a platinum crucible at 1673 K for 300 s in an electric furnace and then poured into a brass mould with thickness of 5 mm. Afterwards, the reduced glass samples were prepared. Industrial mould fluxes usually contain carbon, which can reduce iron oxides in the mould flux. However, the excess graphite powders are known to delay the melting of mould fluxes [12]. Thus, silicon powder was used as the reducing agent in this study. The base glass samples were crushed and mixed with 1 mass% of silicon powder, which was added as the reducing agent in the alumina mortar. The silicon powder used had a median diameter of 5 μm, which was measured using a scanning electron microscope (SEM). The mixture was placed in an alumina crucible, retained at 1703 K for 2–60 min and then poured into the brass mould, which was the same as that for base glass samples. However, the mould in this process was preheated at 723 K for 5 min before moulding to avoid cracking of the glass samples. In these reduction conditions, the main reaction would be the reduction of iron oxide in the melt expressed as follows:

$$2FeO(l) + Si(s) \rightarrow 2Fe(s) + SiO_2(l). \quad (1)$$

The standard Gibbs energy for the above reaction is calculated to be − 444 kJ at 1703 K [12, 13]. By assuming Raoult's rule, the Gibbs energy change (ΔG) was calculated for reaction (1). The result showed a negative value ($\Delta G = -414$ kJ), thereby suggesting that the reaction occurs in the experimental condition.

2.2 Analysis

A spectrophotometer with an integrating sphere covering the wavelength range of 300–2600 nm was used to measure the apparent transmissivity (T_a) and reflectivity (R_a) of the samples. The absorptivity (A_a) was calculated from T_a and R_a.

The sample surface was observed using an optical microscope to identify the particles that were produced via reduction and a digital microscope to count the particles and measure their diameters. The SEM was also used to analyse the size and chemical compositions of the particles by using an energy dispersion spectroscope (EDS). In addition, the electron probe micro-analyser (EPMA) was adopted to examine the chemical composition of the samples. Meanwhile, the transmission electron microscope (TEM) was employed to determine the particles with small sizes.

3 Results

3.1 Appearance of the samples

Figure 1 shows the images of the samples with various reduction time. The sample prior to reduction exhibits a yellowish-green colour. The sample reduced for 2 min did not completely melt. After the reduction, the reduced samples in 5, 10, 15 and 30 min showed black opaque colour and the spheres with metallic lustre were observed with a diameter of 1–3 mm near the surfaces. The samples reduced for 45–60 min had slightly bluish grey colour and showed transparency.

3.2 Optical properties

Figure 2 illustrates the measurement results of R_a, T_a and A_a. The reflectivity is low regardless of the reduction time, that is, nearly 0 prior to reduction and approximately 0.1

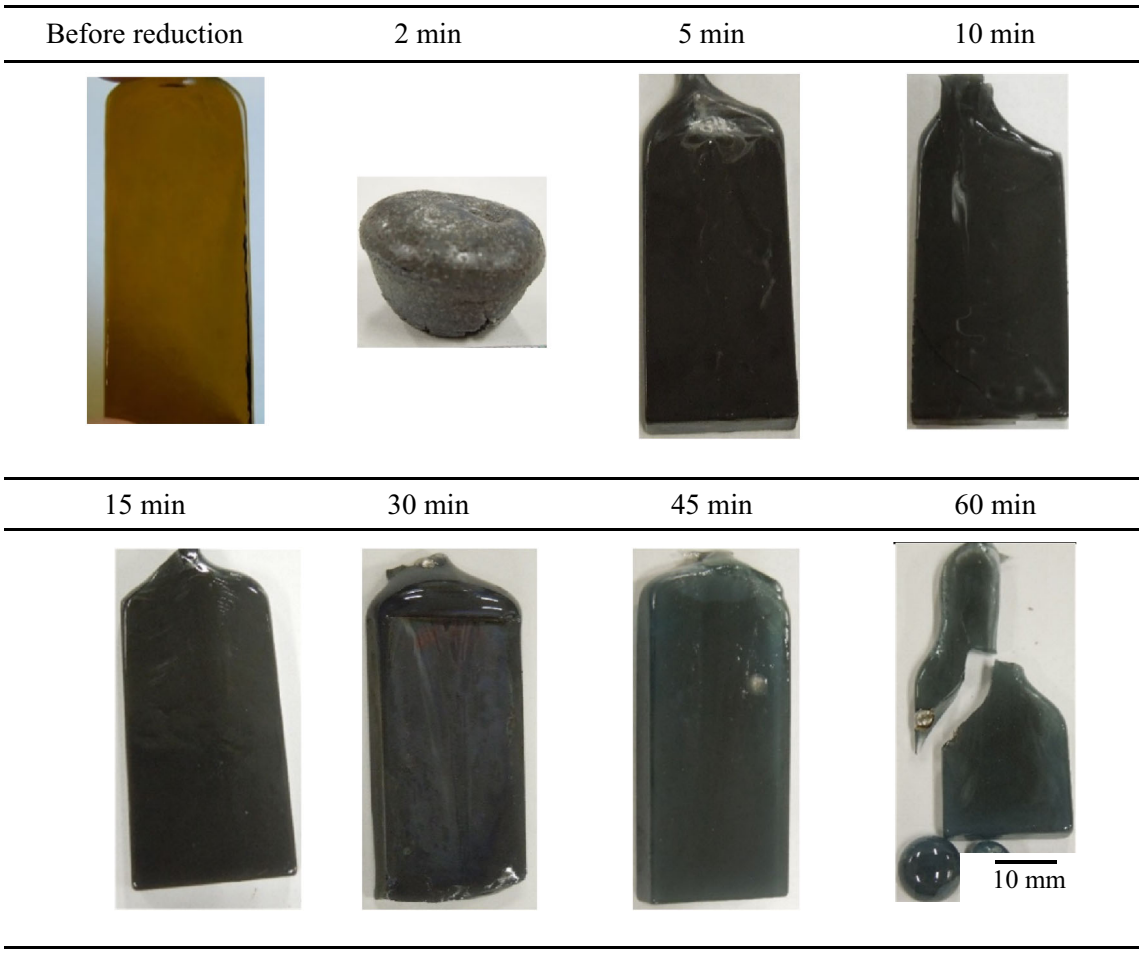

Fig. 1 Photographs of samples

even after the reduction. The absorptivity of the sample prior to reduction exhibits a peak owing to strong absorption by Fe^{2+} and Fe^{3+} in the wavelength range of 500–1000 nm [14, 15]. Meanwhile, all of the reduced samples show a remarkably high absorptivity of approximately 0.9. For the samples reduced for 45–60 min, the transmissivity increases with the reduction time, which is consistent with the appearance of the samples.

3.3 Surface observation

As shown in Fig. 1, the particles of the reduced samples with metallic lustre can be observed with the naked eye. There is also a possibility of smaller particles dispersed in the sample. Figure 3 shows the optical microscope image of the sample reduced for 30 min. Many spherical particles were found with metallic lustre as denoted by arrows. The number and diameter of the metallic particles were analysed using a digital microscope, and the size and area of more than 50 metallic particles were obtained. Figure 4 shows the diameter distribution of the particles in a unit area of 1 mm^2, where the diameter was calculated from the area of the particles. In the 5-min reduced sample, more than 340 particles were determined in the unit area, and the number slightly decreases with reduction time. This finding could be caused by the formation of larger particles similar to the ones observed by the naked eye. After 15 min, the number of particles did not remarkably change. The particles with a diameter of 4–8 μm were mainly found in all the samples in this analysis. Because determining the particles smaller than 1 μm in diameter was difficult with the digital microscope employed in this study, SEM was adopted to analyse smaller particles.

3.4 SEM and TEM analysis

Figure 5 shows the results of the microstructure observation by using SEM for the samples with each reduction time. The sample reduced for 5 min contains many fine metallic particles. The particles obtained were

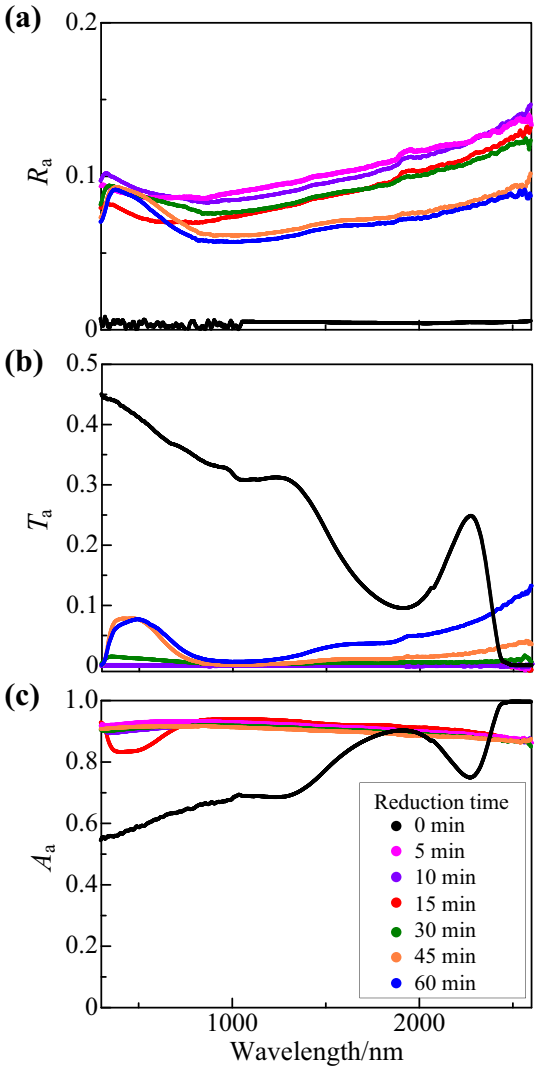

Fig. 2 Result of optical measurement as a function of wavelength. **a** Reflectivity; **b** transmissivity; **c** absorptivity

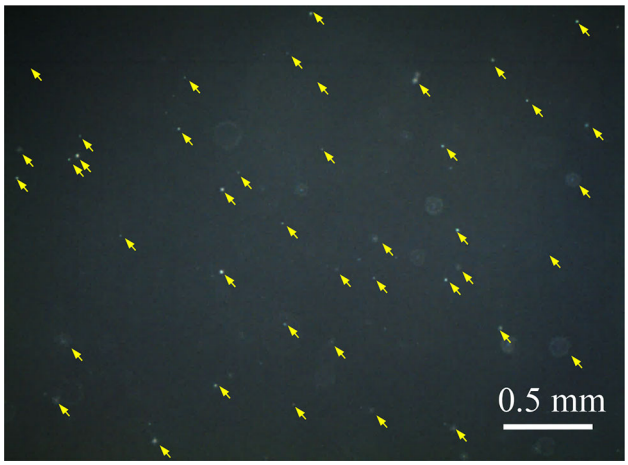

Fig. 3 Optical micrograph of sample retained for 30 min

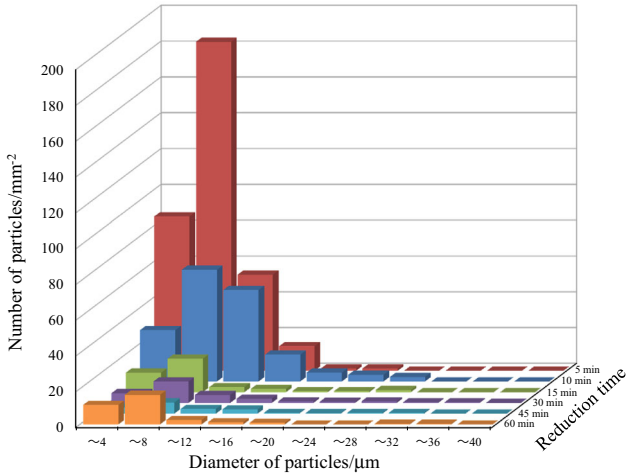

Fig. 4 Size distribution of metallic particles normalised in unit area of 1 mm^2 analysed by using a digital microscope

approximately 0.1 μm in diameter or larger. The metallic particles gradually grew and became more significant with reduction time. Similar to the sample reduced for 30 min, the particles with peanut shape were also observed as denoted by an arrow, in which the particle was formed by attaching 2–4 iron particles, suggesting the formation of large particles through the combination of small particles. Figure 6 shows the number distribution of particles with a diameter of 0.2–8.0 μm. Many particles are found in the diameter of less than 1 μm for the reduced sample in 5 min. Most particles were distributed in a diameter range of less than 3 μm. Figure 4 can be revised to distribute the many particles with a diameter of 4 μm or less by considering Fig. 6. Figures 4 and 6 suggest that many particles were formed during an early stage of the reduction and the number decreased steeply for the formation of large particles. The TEM analysis was also applied, and no iron particles were observed even though several pieces of the samples were analysed.

The chemical compositions of the sample were analysed using SEM–EDS and EPMA. Figure 7a shows an SEM image of a micro-sized metallic particle found in the sample reduced for 30 min. The chemical composition was analysed for both the matrix part and metallic sphere of the sample through the point analysis of EDS. The matrix part is composed of 0.023% Fe, whereas the chemical composition of the metallic particle was 7%Si–93%Fe. The reduction rate was calculated as 96% from the iron concentration in the matrix and initial Fe_2O_3 concentration. This result suggests that almost all Fe_2O_3 was reduced to form metallic particles. Figure 7b shows the concentration of iron in metallic particles as a function of the particle diameter for the 30-min reduced sample. The particles with a diameter smaller than 2 μm cannot be analysed because of the limitation of EDS, and the data obtained for 2 μm

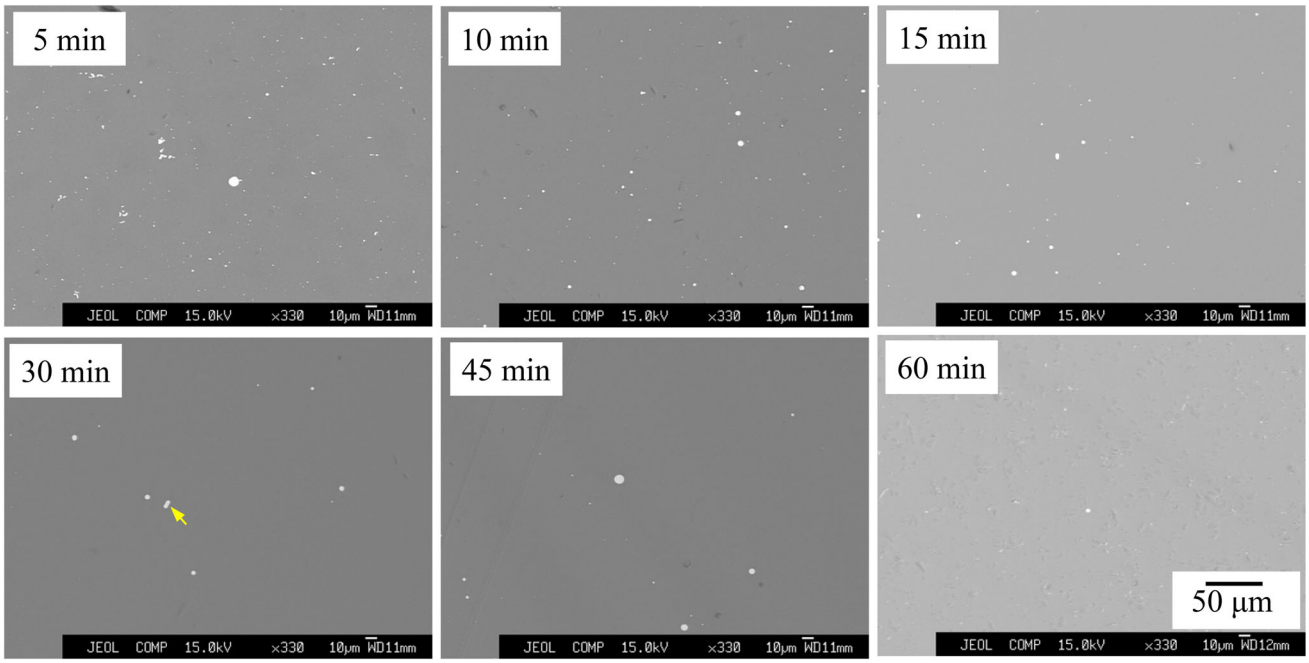

Fig. 5 SEM images for samples with different reduction time

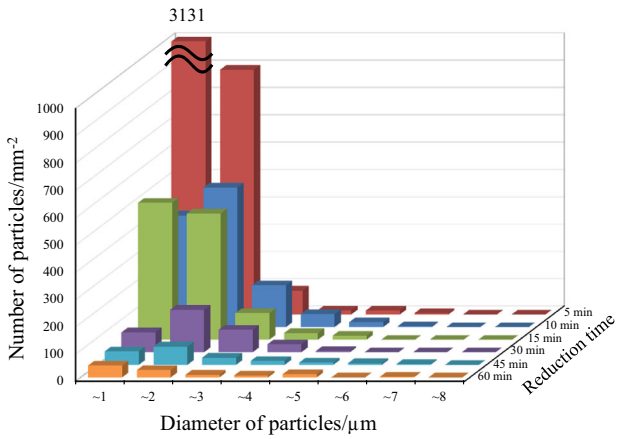

Fig. 6 Size distribution of metallic particles normalised in unit area of 1 mm^2 analysed by using SEM

diameter particles were also considered to contain information from the matrix, which has a smaller Fe concentration than that in metallic particles. This figure suggests that the concentration of Fe is approximately 95% for the particles with diameter of 2–6 μm and decreases with the increasing particle size. The larger particle, which was observed in the 30-min reduced sample with the naked eye, was also analysed using SEM–EDS: the chemical composition was 53%Fe–40%Si composed of O, F, and so on. Figure 8 shows the FeO concentration in the matrix part analysed using the EPMA. The FeO concentration in the matrix decreases with reduction time. After the 15-min reduction, the concentration of FeO is as small as that

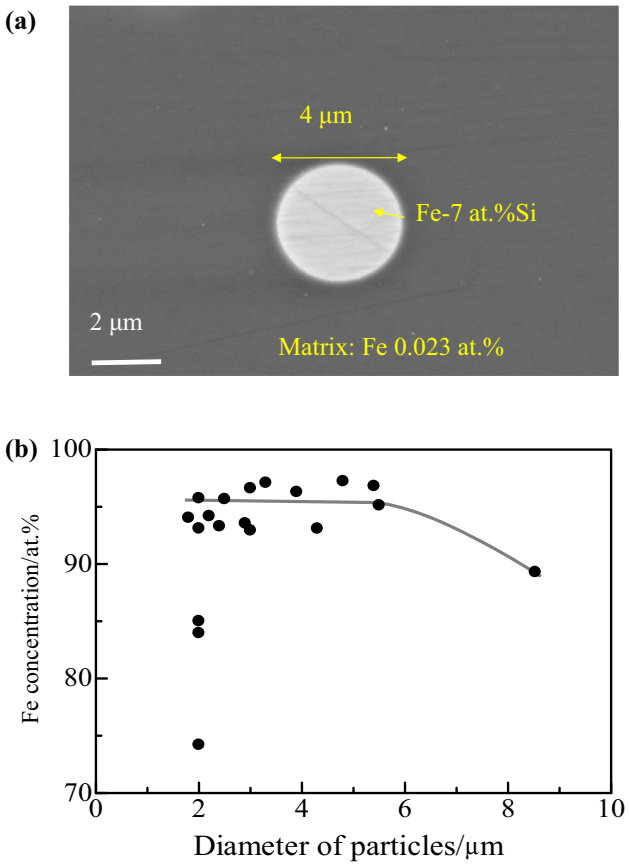

Fig. 7 SEM-EDS results obtained for sample retained for 30 min. **a** Photograph of metallic particle; **b** concentration of Fe in metallic particles as a function of particle diameter

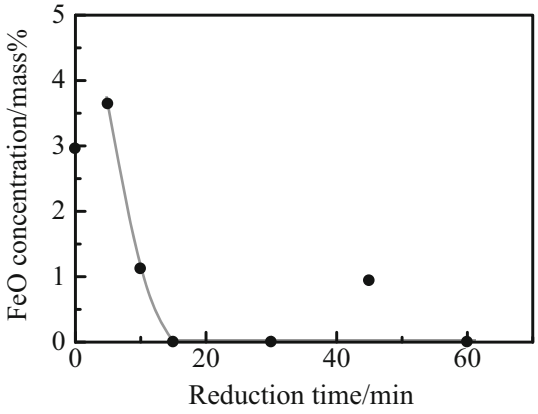

Fig. 8 FeO concentration in matrix analysed by using EPMA

which can be detected using the EPMA, whereas the larger value found in the 45-min reduced sample can be measured because the analysed area contains fine metallic particles. The reduction was considered to be finished within 15 min, and then the particles simply grew with the silicon dissolution.

4 Discussion

4.1 Colouring mechanism of the flux with silicon addition

The above analysis indicates that the metallic particles are iron and the contents of silicon and other elements increase as the particles grow. The reduction is almost finished within 15 min. However, two colours were found after that time, that is, black opaque for 15–30-min reduced samples and transparent bluish grey for 45–60-min reduced samples. The optical property of the samples would have the contribution of the dispersion of micro-sized iron particles. Furthermore, the remaining reduction agent would influence the optical property of samples reduced for 2–30 min.

The colour appearance should be the result of the contributions of (1) the optical interaction between a dispersed particle and the glassy matrix and (2) the dispersed state of the particles. The former can be evaluated from the efficiency of extinction, which is defined as the ratio of the extinction cross section to the geometrical one, for a micro-sized iron particle in a glassy mould flux. The basis of the Mie scattering can be adopted in this situation given that the diameter of iron particles is in the same order with the visible light or the emission peak of molten iron (e.g. 1.6 μm at 1800 K). The software 'MiePlot' [16] was adopted to calculate the scattering efficiency of an iron particle. Figure 9 shows the efficiencies of extinction, scattering and absorption for the Fe particle at the

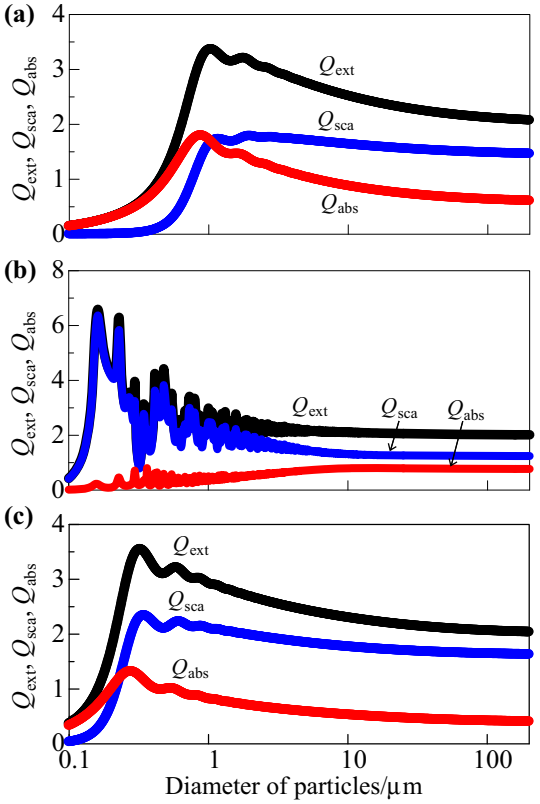

Fig. 9 Efficiencies of extinction (Q_{ext}), scattering (Q_{sca}) and absorption (Q_{abs}) of Fe particle at 0.65 μm (**a**), Si particle at 0.65 μm (**b**) and Fe particle at 1.60 μm (**c**) in mould flux as functions of particle diameter

wavelength of 0.65 μm, Si particle at 0.65 μm and Fe particle at 1.60 μm in mould flux as diameter functions of the particle. The wavelengths of 0.65 and 1.60 μm are representatives for the visible region and emission peak at 1800 K, respectively. In this calculation, the refractive indexes used for Fe and Si were from the recommended values of Palik [17] as well as Aspnes and Studna [18], respectively. In addition, the refractive index for the reduced mould flux was calculated on the basis of the optical property data reported for the mould flux without iron oxide [1]. The data used for this calculation are listed in Table 1. As shown in Fig. 9a, the scattering efficiency for extinction, which is the sum of the scattering and absorption, increases with the increasing particle size up to 1 μm and then decreases gradually. Hence, both scattering and absorption contribute to this result. These scattering or absorption processes are valid for the samples in this study given that the diameter of iron particles is in the micrometre order. Figure 9b suggests that the scattering has a larger effect than absorption in the case of silicon dispersion at 0.65 μm. The calculation result at 1.60 μm is also shown in Fig. 9c. The same result was obtained; that is, the scattering and absorption efficiency are strong for

Table 1 Refractive index used for calculation

Wavelength/μm	Fe [17]	Si [18]	Mould flux (without iron oxide) [1]
0.65	2.9114	3.8515	1.4843
1.60	3.1091	–	1.4932

iron particles of more than 0.3 μm in diameter. However, the scattering is more effective than the absorption. The calculations for Fig. 9 are for one particle in the mould flux. In reality, many particles dispersed in the mould flux sample and scattered light are possibly scattered again or absorbed by iron particles. Figure 10 shows the number of particles formed in a unit area within the diameter range of 0.7–10 μm with various reduction time. The number of iron particles dramatically decreased with the holding time up to 30 min, after which time the number change becomes slow. The number of iron particles has no apparent difference between the samples reduced for 30–45 min. However, the former sample had the black opaque colour, whereas the latter showed transparent bluish grey. Therefore, the remaining silicon would affect the colour of the 30-min reduced sample. The assumption can be supported by the report of Yoon et al. [19, 20]. They used the iron particle dispersed mould flux of the borosilicate system to measure the heat flux across the flux. The diameter of the iron particle was lower than 3 μm, which is almost the same as that in this study. In their report, the absorption coefficient of the sample increased with the increasing Fe particle content. However, the black opaque colour has not been found, and only the green colour was observed owing to the absorption of iron oxides. As shown in Fig. 2, the strong absorption of all the reduced samples could be due to the absorption by micro-sized Fe particles with scattering of Si or Fe particles. The former process would be more effective in the samples reduced for 2–30 min, resulting in the black opaque colour. The important point would be not the appearance of the colour in visible light, but the high absorptivity in the near-infrared light because the radiative heat transfer is related to the near-infrared light.

4.2 Evaluation of apparent thermal conductivity of black opaque mould flux

The apparent thermal conductivity of solid mould flux, which has contributions both from conduction and radiation, was calculated on the basis of the heat resistance model [21–23], as shown in Fig. 11. The mould flux consists of liquid, crystallised and glassy layers. The solid layer has a mild cooling property. Thus, the thermal conductivity of solid flux was estimated in this section. In this calculation, the heat flux of both radiation and conduction was obtained in each layer, and the sum of the heat fluxes (q_{total}) was considered to be equal in each layer under steady state, as expressed using the following equations:

$$q_{\text{total}} = q_{\text{r,crys}} + q_{\text{c,crys}}, \tag{2}$$

$$q_{\text{total}} = q_{\text{r,glass}} + q_{\text{c,glass}}, \tag{3}$$

where q represents heat flux; and the subscripts r, c, crys and glass represent radiation, conduction, crystallised and glassy, respectively. The heat fluxes by conduction and radiation in each layer are expressed in the following equations, respectively:

$$q_{\text{c}} = \lambda_{\text{c}}\left(\frac{T_{\text{I}} - T_{\text{II}}}{d}\right), \tag{4}$$

$$q_{\text{r}} = \frac{n^2\sigma\left(T_{\text{I}}^4 - T_{\text{II}}^4\right)}{0.75\alpha d + \varepsilon_{\text{I}}^{-1} + \varepsilon_{\text{II}}^{-1} - 1}, \tag{5}$$

where λ_{c}, α, n, σ, d, ε and T are thermal conductivity by conduction, absorption coefficient or extinction coefficient,

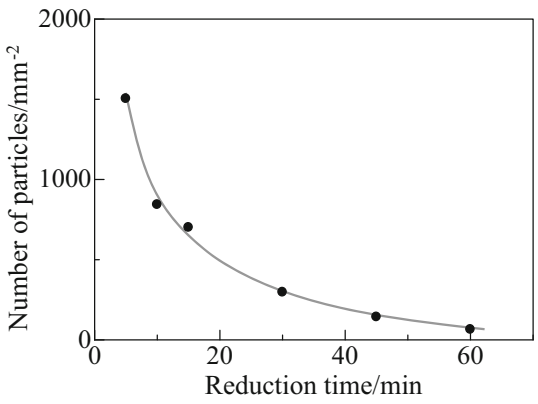

Fig. 10 Number of particles with diameter of 0.7–10 μm with reduction time. SEM analysis data were used for this analysis

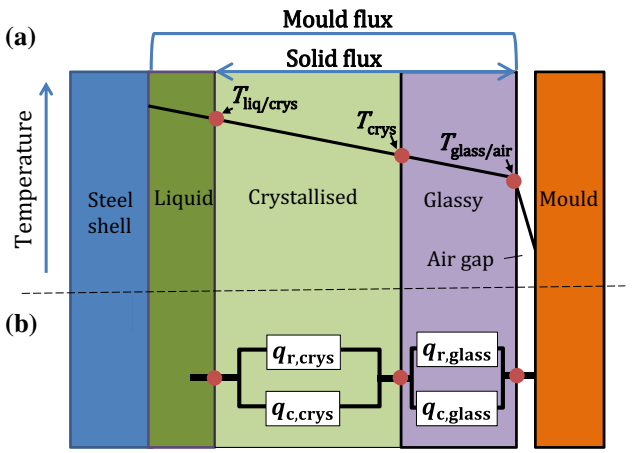

Fig. 11 Schematic of temperature distribution (**a**) and calculation model (**b**) applied in this study

refractive index, Stefan–Boltzmann's constant, layer thickness, emissivity and temperature, respectively; and the subscripts I and II are high and low temperatures of the considered layer, respectively. The temperatures at the interfaces were set to 1388 K at liquid/crystallised mould flux ($T_{liq/crys}$) [21], crystallisation temperature (T_{crys} = 823 K) at the crystallised/glassy flux used in this study [23] and 772 K at glassy flux/air gap ($T_{glass/air}$) [21]. The total thickness of solid mould flux (d_{total}) was set to 1 mm [21, 22]. By substituting these parameters into Eqs. (2)–(5) with the thermophysical properties listed in Table 2, the thickness of the layers and heat fluxes can be derived, thus reproducing the apparent thermal conductivity of solid flux (λ_{app}) from the following equation.

$$q_{total} = -\lambda_{app}\left(\frac{T_{liq/crys} - T_{glass/air}}{d_{total}}\right) \quad (6)$$

The calculation was performed for the conventional solid and 30-min reduced mould flux, both of which consist of crystallised and glassy layers. Moreover, the completely glassy reduced mould flux was considered. The thermophysical properties listed in Table 2 were determined as follows. The values of the conventional flux refer to the data reported for the mould flux with similar composition as this research. The value of α (glassy) for the reduced flux was derived from the transmissivity of the 30-min reduced sample in the wavelength range of 1.0–2.6 μm, as shown in Fig. 2b with the Lambert–Beer's law. The value of α (crystallised) was set to be equal to α (glassy) for the reduced sample [11]. The emissivity at the interface related to the crystallised phase (ε (liquid/crystallised) and ε (crystallised/glassy)) was considered as a unit because the interface would be rough owing to fine crystal formation. The emissivity at the interface between the glassy flux and air gap (ε (glassy/air gap)) was derived from the absorptivity of the glassy flux. The value of ε (liquid/glassy) was also obtained from the absorptivity of the glassy flux, because the liquid flux may have the same optical property.

Table 2 also shows the calculation results of λ_{app} and thickness of the glassy layer (d_{glass}). The reduced mould flux shows smaller λ_{app} than the conventional one. Both crystallised fluxes have high absorption coefficient owing to the high crystallinity of metallic particles for the conventional and existing one and high crystallinity of the reduced one, respectively. High absorptivity resulted in almost the same heat transfer characteristics in the conventional and reduced fluxes. Meanwhile, the high absorptivity of the reduced flux has effects on the heat transfer in the glassy layer. The thickness of the glassy layer increased with the high absorptivity of the reduced glassy flux, resulting in low apparent thermal conductivity. However, the glassy layer must be too thin (i.e. only 5% in the total thickness) to decrease the apparent thermal conductivity dramatically. The apparent thermal conductivity would effectively decrease for the flux with high crystallisation temperature. In this extreme case, the mould flux becomes completely glassy. Table 2 also shows the calculation results of the completely glassy mould flux. The value of λ_{app} is 19% smaller than that of the conventional mould flux because of the small lattice thermal conductivity apart from the large absorptivity. In addition, the temperature of the interfaces may possibly change depending on the flux characteristics. However, the effectiveness of the completely glassy flux is considered to be sufficient to reduce the apparent thermal conductivity. To demonstrate the effectiveness of the completely glassy mould flux with high absorptivity, further measuring the heat flux of the mould flux experimentally is necessary.

Table 2 Thermophysical properties used for model calculation, derived apparent thermal conductivity of solid mould flux and thickness of glassy layer

Parameter	Conventional	Reduced	Reduced (completely glassy)
α (crystallised)/m^{-1}	907 [1]	1090	–
α (glassy)/m^{-1}	166 [1]	1090	1090
n (crystallised)	1.59 [21, 24, 25]	1.59 [21, 24, 25]	–
n (glassy)	1.58 [21, 24, 25]	1.58 [21, 24, 25]	1.58 [19, 22, 23]
λ (crystallised)/(W m^{-1} K^{-1})	1.59 [21, 23]	1.59 [21, 23]	–
λ (glassy)/(W m^{-1} K^{-1})	1.25 [11, 21]	1.25 [11, 21]	1.25 [11, 21]
ε (liquid/crystallised)	1	1	–
ε (crystallised/glassy)	1	1	–
ε (glassy/air gap)	0.527	0.9	0.9
ε (liquid/glassy)	–	–	0.9
λ_{app}/(W m^{-1} K^{-1})	2.00	1.97	1.62
d_{glass}/mm	0.051	0.053	1

4.3 Further utilisation of mould flux with high absorptivity

In this section, the application of silicon mixture in conventional mould flux will be discussed. In the actual continuous casting process, the mould flux melts in the slag pool and infiltrates between the steel shell and mould, thus forming a slag film. The slag film usually consists of liquid, crystallised and glassy layers [22, 24]. The casting speed is typically reported to be 1–3 m/min, thereby suggesting that the slag film passes through the caster in no more than 30 min. Considering the silicon addition to the mould flux powder, the mould flux with high absorptivity would only form after the flux melts, and the high absorptivity can be retained in the caster. The same results can be expected with the addition of 0.5% Si or more because Wang et al. [11] reported that the mould flux with high absorptivity can be produced by the addition of 0.5–5.0% Si after the 30-min melting at 1703 K. Scheller et al. [26, 27] also reported the formation of metallic spheres in the mould flux, which is used for the casting of stainless steel. In this report, the metallic particles act as the nucleation sites of the mould flux crystallisation. Mild cooling by the flux with high absorptivity would be realised by utilising such metallic particles to control the heat flux across the mould flux. In addition, the effect of small metallic particles in the slag on the viscosity must also be considered because the mould flux has other functions for the steel casting, such as lubrication, and the particle dispersion is expected to increase the viscosity [28].

5 Conclusions

The silicon addition to mould flux resulted in all the samples having high absorptivity (~ 0.9) by reducing them at 1703 K for 2–60 min. The mould flux with black opaque colour was found after the 5–30-min reduction. The samples reduced for 45–60 min became transparent bluish grey. Many iron-based particles were found in the micrometre order of all the samples. The reduction was almost finished within 15 min, and then iron particles grew by combining several particles. The Mie scattering occurred in the samples, and the scattering process became efficient in the 5–30-min reduced samples by using the remaining silicon. The iron particles in micrometre order effectively absorb the scattered light, resulting in the high absorptivity of all the samples.

The mould flux with high absorptivity was assumed not to change the apparent thermal conductivity of the conventional mould flux, which was oriented to crystallise. Meanwhile, the completely glassy mould flux with high absorptivity had smaller apparent thermal conductivity, thereby suggesting the mild cooling possibility of continuous casting.

Acknowledgements This work was partially supported by a research grant from the Technical Association of Refractories, Japan.

References

[1] M. Susa, A. Kushimoto, H. Toyota, M. Hayashi, R. Endo, Y. Kobayashi, ISIJ Int. 49 (2009) 1722–1729.
[2] K.C. Mills, A.B. Fox, ISIJ Int. 43 (2003) 1479–1486.
[3] S. Harada, S. Tanaka, H. Misumi, S. Mizoguchi, H. Horiguchi, ISIJ Int. 30 (1990) 310–316.
[4] Y.M. He, Q. Wang, B. Hu, L.L. Zhu, W.M. Chen, S.P. He, Ironmak. Steelmak. 43 (2016) 588–593.
[5] A.I. Zaitsev, A.V. Leites, A.D. Lrtvina, B.M. Mogutnov, Steel Res. 65 (1994) 368–374.
[6] Y. Kashiwaya, A.W. Cramb, Metall. Mater. Trans. B 32 (2001) 401–407.
[7] M. Persson, S. Seetharaman, S. Seetharaman, ISIJ Int. 47 (2007) 1711–1717.
[8] A.F. Dick, X. Yu, R.J. Pomfret, K.S. Coley, ISIJ Int. 37 (1997) 102–108.
[9] S. Dević, L. Marčeta, Am. Ceram. Soc. Bull. 86 (2007) 9101–9103.
[10] B. Walna, I. Kurzyca, E. Bednorz, L. Kolendowicz, Environ. Monit. Assess. 185 (2013) 5497–5514.
[11] M. Wang, R. Endo, Y. Kobayashi, Y. Susa, M. Susa, M. Hanao, Journal of the Technical Association of Refractories, Japan (Taikabutsu Overseas), 36 (2016) 3–9.
[12] M. Kawamoto, K. Nakajima, T. Kanazawa, K. Nakai, ISIJ Int. 34 (1994) 593–598.
[13] I. Barin, Thermochemical data of pure substances, 3rd Ed., Weinheim (Germany), 1995.
[14] M. Susa, K. Nagata, K.C. Mills, Ironmak. Steelmak. 20 (1993) 372–376.
[15] Y. Kobayashi, R. Maehashi, R. Endo, M. Susa, ISIJ Int. 53 (2013) 1725–1731.
[16] P. Laven, MiePlot, http://www.philiplaven.com/MiePlot.htm [accessed: 10.07.2017].
[17] E. Palik, Handbook of optical constants of solids: Volume 1, Academic Press, Boston, 1985.
[18] D.E. Aspnes, A.A. Studna, Phys. Rev. B 27 (1983) 985–1009.
[19] D.W. Yoon, J.W. Cho, S.H. Kim, Metall. Mater. Trans. B 47 (2016) 2785–2792.
[20] D.W. Yoon, J.W. Cho, S.H. Kim, Metall. Mater. Trans. B 48 (2017) 1951–1961.
[21] H. Nakada, M. Susa, Y. Seko, M. Hayashi, K. Nagata, ISIJ Int. 48 (2008) 446–453.
[22] M. Hanao, M. Kawamoto, A. Yamanaka, ISIJ Int. 52 (2012) 1310–1319.
[23] S. Takahashi, R. Endo, T. Watanabe, M. Hayashi, M. Susa, ISIJ Int. 58 (2018) 905–914.
[24] K.C. Mills, ISIJ Int. 56 (2016) 1–13.
[25] M. Susa, K.C. Mills, M.J. Richardson, R. Taylor, D. Stewart, Ironmak. Steelmak. 21 (1994) 279–286.
[26] P.R. Scheller, High Temp. Mat. Pr-Isr. 22 (2003) 387–394.
[27] P.R. Scheller, Y. Lin, Q. Shu, in: Proc. of the 7th International Congress on Science and Technology of Steelmaking (ICS 2018), Associazione Italiana di Metallurgia, Milano, 2018, ICS_235.
[28] N. Saito, S. Yoshimura, S. Haruki, Y. Yamaoka, S. Sukenaga, K. Nakashima, Tetsu-to-Hagané 95 (2009) 282–288.